Technical Simulation for the Hydromagnetic Rotating Flow of Carreau Fluid with Arrhenius Energy and Entropy Generation Effects: Semi-Numerical Calculations

[1] M. G. IBRAHIM, [2]HANA ABDELHAMEED ASFOUR
[1]Basic and Applied Science Department, International Academy for Engineering and Media Science, 11311, Cairo, EGYPT
[2]Basic and Applied Science Department, Thebes Academy, 11311, Cairo, EGYPT

Abstract: - The present study aimed to investigate the influence of activation energy on the MHD Boundary layer of Carreau nanofluid using a semi-numerical/analytical technique. The governing formulated system of partial differential equations (PDEs) subject to appropriate boundary conditions is shortened to ordinary differential equations (ODEs) by convenient transformations. Generalized Differential Transform (GDTM) is used and compared with the Runge–Kutta Dahlberg method to find the results of the proposed system. GDTM is chosen to cure and overcome the highly non-linear differentiation parts in the present system of ODEs. Gradients of velocity, temperature, and concentration are computed graphically with different values of physical parameters. The solutions are offered in two cases, the first in the case of non-Newtonian fluid (We=0.2) and the other in the case of base fluid (We=0.2), which is concluded in the same figure. The accuracy of GDTM is tested with many existing published types of research and found to be excellent. It is worth-mentioned that the distribution of velocity growths at high values of power index law relation. This fluid model can be applied in solar energy power generation, ethylene glycol, nuclear reactions, etc.

Key-Words: - Activation energy; Boundary layer; GDTM; Entropy Generation; Carreau nanofluid.

Received: August 18, 2021. Revised: October 14, 2022. Accepted: November 17, 2022. Published: December 31, 2022.

1 Introduction

Non-Newtonian fluids studies captured the attention of scholars and researchers in the last years, because of their engineering and industrial applications in various fields. These applications like cosmetics, molten polymers, food products, oils, certain paints, drilling mud, fluid suspensions, volcanic lava, etc.… Interests of scholars/researchers increase with the stress tensor in such fluids which accompany the deformation rate tensor by relationships of highly nonlinear differentiation. This non-linear mechanism of non-Newtonian fluids gives rise to complicated non-linear equations. Ghasemi and Hatami, [1] scrutinized the solar effects on the MHD boundary layer flow of a nanofluid; they found that the distribution of velocity is an increasing function in heat generation. Khalil et al,. [2] deliberated the Eyring-Powell fluid with an inclined stretching cylinder. Shafiq and Sindhu, [3] suggest a new radiative effect on the flow of a non-Newtonian fluid. Mabood et al, [4] deliberated the heat and generation effects on the flow of Hybrid fluid. Shafiq et al [5] and Zari et al [6] studied new effects of Darcy and MHD effects on the Casson flow with nanoparticles. Malik et al, [7] scrutinized the numerical investigation of paramount non-Newtonian fluid on a sheet. There are many papers introduces a non-Newtonian fluids and its applications, [8-14]. In physics and fluid mechanics, the boundary layer constitutes an important concept and refers to the fluid layer near an ocean surface where viscosity effects are significant. Even in the flow where viscosity is low and can be ignored, there is a thin film whose viscosity cannot be ignored at a boundary such as an object surface or wall surface, this layer is called the boundary layer. Since the actual liquid is viscous, the relative velocity is 0 at the boundary between the liquid and the wall. Ideal with viscosity set to ideal fluids although the theory is mathematically brief when dealt with, the state of the adhesive cannot be satisfied, and the sliding velocity parallel to the wall is generally shown. Also, in an ideal fluid, the resistance acting on a body moving at a constant velocity in it becomes zero. The boundary layer idea was introduced by L. Prandtl in 1904, [15] to mitigate these contradictions and lay the foundation for modern fluid dynamics. A timed method on boundary layer flow problems was addressed by Pasha et al, [16], they found that radiation flux is an increasing function in heat transfer. Khan et al, [17] studied the influences of solar radiation and heat generation on non-Newtonian nanofluid over a stretching sheet with variable thickness, they found that the temperature distribution is enhanced at high values of heat generation. In chemistry and physics, activation energy is the energy that must be supplied to a chemical or nuclear system of latent reactants that lead to a chemical reaction, a nuclear reaction, or various other physical phenomena. It is denoted by the symbol, and the unit kilojoule/mole is used to measure it. The term was coined by the Swedish chemist Svante Arrhenius in 1889, [18]. Shafique et al, [19], discretized the influences of activation energy on boundary layer flow in a rotating frame; they found that the activation energy is an increasing function in the temperature of the fluid. Gowda et al, [20], studied the heat and mass transfer effects on the boundary layer of non-Newtonian fluid, they found that the growing values of the magnetic parameter develop the velocity gradient and decay the heat transfer. In nearly times, applications of activation energy appeared more and more in different fields like nuclear reactions in engineering, [21], various physical phenomena in physics, [22,23], and many applications can be found in [24 − 28]. The current scientific eagerness to find new numerical, semi-numerical, and analytical methods for finding the solutions to fluid problems that have a high degree of nonlinearity is in the interest of mathematics sciences. One of the methods that appeared to solve the problem of nonlinearity in partial or ordinary differential equations is called the generalized differential transform method, which is shortened to GDTM as offered in this manuscript. The differential transform method was first introduced at the end of the last century by Zhou, [29], which is defined as a semi-analytical method for solving nonlinear partial differential equations. In early times, Odibat et al [30] studied the non- non-chaotic or chaotic systems by using a new modified technique called the multi-step differential transform algorithm. Also, a large number of investigations have proven the effectiveness of the DTM and its modification techniques, [31 − 44]. On another side, the main idea for GDTM is to choose/ divide a suitable number of intervals from solution intervals, as well as make a generalization of the resulting differential transform series solution. To illustrate the GDTM in detail, section 3 is made to compute the graph solutions of the MHD boundary layer flow of Carreau nanofluid.

The main novelty of this paper is to introduce a new simulation of the Arrhenius activation energy of the hydromagnetic rotating flow of Carreau fluid entropy generation effects using GDTM. Combined solutions of the proposed model in the cases of Newtonian and non-Newtonian fluid are discussed to clarify the fluid behaviors. Comparisons have been made with previously existing published results by Khan et al, [24], Wang, [25], Gorla and Sidawi, [26], and Mabood et al, [27], and found to be in good agreement. In addition, comparisons of temperature and concentration distributions have been made with results given by Khan et al, [24] and found to be excellent as stated/indicated. In the next subsection, the formulation of the problem is introduced; in section 3, the generalized method is presented; discussions of the graphed results are offered in section 4; eventually, the conclusion and main points are concluded in the last section of the current paper.

2 Mathematical Formulations

The boundary layer flow of Carreau nanofluid with variable thickness is considered as a mathematical system of differential equations $y = B(x+b)^{\frac{1-m}{2}}$ is to be assumed the thickness of the sheet, where b is constant and m is the index of the power law. The magnetic field $B_0(x)$ is supposed to vary with the strength and vertical to plate as shown in $\boldsymbol{Fig.1}$.

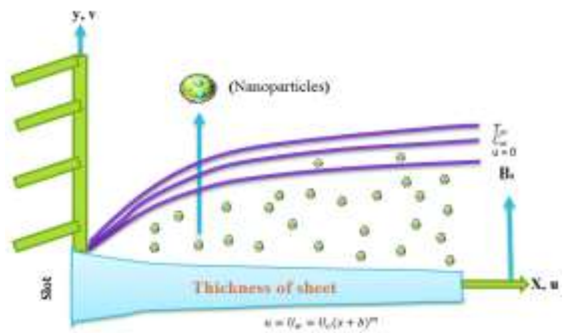

Fig. 1: Geometry of physical model

The Carreau nanofluid combined with the boundary layer approximation mode l is written as:

$$\frac{\partial u'}{\partial x'}+\frac{\partial v'}{\partial y'}=0, \tag{1}$$

$$u'\frac{\partial u'}{\partial x'}+v'\frac{\partial v'}{\partial y'}=\left(u'\frac{\partial^2 u'}{\partial x^{2'}}+v'\frac{3(n-1)}{2}\Gamma^2\left(\frac{\partial u'}{\partial y'}\right)^2\frac{\partial^2 u'}{\partial y^{2'}}\right)-\frac{\sigma B_0^2 u'}{\rho}, \tag{2}$$

$$\rho c_p\left(u'\frac{\partial T'}{\partial x'}+v'\frac{\partial T'}{\partial y'}\right)=\alpha\frac{\partial^2 T'}{\partial y^{2'}}+\tau\left\{D_B\left(\frac{\partial T'}{\partial y'}\frac{\partial C'}{\partial y'}\right)+\frac{D_{T'}}{T'_\infty}\left(\frac{\partial T'}{\partial y'}\right)^2\right\}-\frac{\partial q_r}{\partial y}+Q_0\left(T'-T'_\infty\right), \tag{3}$$

$$u'\frac{\partial C'}{\partial x'}+v'\frac{\partial C'}{\partial y'}=D_B\left(\frac{\partial^2 C'}{\partial y^{2'}}\right)+\frac{\rho_p D_{T'}}{M_P T'_\infty}\left(\frac{\partial^2 T'}{\partial y^{2'}}\right)-K_r^2\left(C'-C'_\infty\right)\left(\frac{T'}{T'_\infty}\right)^n e^{\left(\frac{-E_a}{K_B T'}\right)}, \tag{4}$$

The appropriate boundary conditions for Carreau nanofluid are chosen as follows:

$$u\left(x+B(x+b)^{\frac{1-m}{2}}\right)=U_0(x+b)^m, v\left(x+B(x+b)^{\frac{1-m}{2}}\right)=0, T\left(x+B(x+b)^{\frac{1-m}{2}}\right)=T_w, \tag{5}$$

$$u(x,\infty)=0, T\to T_\infty, C\to C_\infty, \text{as } y\to\infty. \tag{6}$$

Here $c_p, T, \rho, Q_0, C, q_r$ and α are the specific heat, the temperature of the fluid, the fluid density, the heat generation, the concentration of fluid, the radiative heat flux and the electric conductivity, respectively. (u, v) are the components along (x, y) direction, D_T and ν are the thermophoretic diffusion coefficient and the kinematic viscosity. C_w and C_∞ are the near and distant away concentrations, B_0 is the applied magnetic field. A similarity transformation is introduced as the following.

By using self-similarity transformations

$$\eta=y\sqrt{U_0\left(\frac{m+1}{2}\right)\left(\frac{(x+b)^{m-1}}{v}\right)}, \Psi=\sqrt{vU_0\left(\frac{2}{m+1}\right)(x+b)^{m-1}F(\eta)},\ \Theta(\eta)=\frac{T'-T'_\infty}{T'_w-T'_\infty}, \Phi(\eta)=\frac{C'-C'_\infty}{C'_w-C'_\infty}, \tag{7}$$

By using transformations in Eq. (7), the system of Eqs. (1-4) with boundary conditions (5-6) become

$$f'''(\eta)+\beta f'^2-f(\eta)f''(\eta)+\frac{3(n-1)}{2}W_e^2 f'^2(\eta)f'''(\eta)-Mf'(\eta)=0, \tag{8}$$

$$\frac{1+R}{P_r}\theta''(\eta)+\theta'(\eta)f(\eta)+N_b\,\theta'(\eta)\phi(\eta)+N_t\left(\theta'(\eta)\right)^2+\gamma\,\theta(\eta)=0, \tag{9}$$

$$\phi''(\eta)+L_eP_rf(\eta)\phi'(\eta)+\frac{N_t}{N_b}\theta''(\eta)-P_rL_e\sigma\left(1+\delta\,\theta(\eta)\right)^n e^{\left(\frac{-E}{1+\delta\,\theta(\eta)}\right)}\phi(\eta)=0 \tag{10}$$

The transformed boundary conditions are

$$f(\eta)=0, f'(\eta)=1, \theta(\eta)=1, \phi(\eta)=1, \eta\to 0,$$
$$f(\infty)=0, \theta(\infty)=0, \phi(\infty)=0, \tag{11}$$

Here, $\beta=\frac{2m}{m+1}$ and,

The Hartmann number

$$M=\frac{2\sigma B_0^2}{(m+1)\rho c_p U_0 (x+b)^{m-1}}, \tag{12}$$

The Weissenberg number:

$$W_e=\frac{U_0^3(x+b)^{3m-1}}{2v}\Gamma^2(m+1), \tag{13}$$

The Prandtl number:

$$P_r=\frac{\mu c_p}{k}, \tag{14}$$

The heat generations parameter:

$$\gamma=\frac{2Q_0(x+b)^{m-1}}{(1+m)\rho c_p U_0}, \tag{15}$$

The Brownian motion parameter:

$$N_b=\frac{D_B(C_w-C_\infty)}{v}, \tag{16}$$

The thermophoresis parameter:

$$N_t=\frac{D_t(T_w-T_\infty)}{v}, \tag{17}$$

The chemical reaction species:

$$\sigma=\frac{k_r^2}{a}, \tag{18}$$

Thermal radiation (heat flux) parameter:

$$R=\frac{4\,\sigma^* T_\infty^3}{K_\infty k^*}, \tag{19}$$

The Lewis number:

$$L_e = \frac{\nu}{D_B}, \tag{20}$$

The temperature difference parameter:

$$\delta = \frac{T'_w - T'_\infty}{T'_\infty}, \tag{21}$$

The Activation energy:

$$E = \frac{E_a}{K_B T'}, \tag{22}$$

3 GDTM Applications

The solution of a system of differential equations (8-10) with boundary conditions (11) using the GDTM is presented in this section in detail. The solution of the proposed system is illustrated step by step to show the quality of the technique with aid of $Mathematica$ 13.0.1.

The first step mentioned the system of differential equations written at the start of Mathematica algorithms. In the same step, we choose the appropriate limit to the solution at the point at which solutions are proven and do not change, no matter how much this value increases. *In the second step*, we transform the system of equations (8-10) with boundary conditions (11) using the differential transform technique [30 − 34] as follows:

$$(k+1)(k+2)(k+3)F[k+3] + \beta \sum_{s=0}^{k}(s+2)(s+1)F[s+2]F[k-s] - \sum_{s=0}^{k}(s+1)k(k-s+1)F[s+1]F[k-s+1] + \frac{3(n-1)}{2} W_e^2 \sum_{s=0}^{k}(s+1)(k-s+1)(k-s+2)F[s+1]F[k-s+1]F[k-s+2] - M(k+1)F[k+1] = 0 = q_1, \tag{23}$$

$$\frac{1+R}{P_r}(k+1)(k+2)\Theta[k+2] + \sum_{s=0}^{k}(s+1)(s+2)\Theta[k-s]F[s+1] + N_b \sum_{s=0}^{k}(s+1)(s+2)\Theta[k-s]\Phi[s+1] + N_t \sum_{s=0}^{k}(s+2)(s+1)\Theta[s+1]\Theta[k-s] + \gamma\,\Theta[k] = 0 = q_2, \tag{24}$$

$$(k+1)(k+2)\Phi[k+2] + L_e P_r \sum_{s=0}^{k}(s+1)(s+2)F(s+1)\Phi[k-s] + \frac{N_t}{N_b}(k+1)(k+2)\Theta[k+2] - P_r L_e \sigma E\,\Phi[k] - 2P_r L_e \sigma\,\mathrm{E}\,\delta \sum_{s=0}^{k}(s+1)(s+2)\Theta[s+1]\Phi[s+2] - P_r L_e \sigma\, E\, \delta^2 \sum_{s=0}^{k}(s+1)(k+s+1)\,\Theta[k+s+1]\Phi[s+1] = 0 = q_3. \tag{25}$$

With transformed boundary conditions using theories of DTM as:

$$F[0]=0, F[1]=1, \Theta[0]=1, \Phi[0]=1, \sum_{r=0}^{k} F_k[\eta_\infty]^k = 0\,, \sum_{r=0}^{k} \Theta_k[\eta_\infty]^k = 0\,, \sum_{r=0}^{k} \Phi_k[\eta_\infty]^k = 0 \tag{26}$$

In the third step, we make a table of differential operations for each variable according to the degree of differentiation for each variable as an algorithm in *Mathematica* (suppose the numberof required solution equal 10, that chosen as we need)

$$\mathbf{S1 = Table[D[q1,\{y,k\}] == 0, \{k,0,7\}]/.\,ss/.\,q_{01};}$$
$$\mathbf{S2 = Table[D[q2,\{y,k\}] == 0, \{k,0,8\}]/.\,ss/.\,q_{01};}$$
$$\mathrm{S3 = Table[D[q3,\{y,k\}] == 0, \{k,0,8\}]/.\,ss/.\,q_{01};} \tag{27}$$

Where the value of k represents the number of solutions to be found, q_{01} is defined as values of non-dimensional parameters, q_1, q_2 and q_3 refer to the system of equations, respectively. *In the fourth step*, we introduce the initial values to the solutions and make a table of contents for the required solutions as follows:

$$U[0] = \{\mathrm{Table}[F_n,\{n,0,3\}], \mathrm{Table}[\Theta_n,\{n,0,1\}], \mathrm{Table}[\Phi_n,\{n,0,1\}]\}/.\,\mathrm{Q0//Flatten} \tag{28}$$

$$\{F[0]=0, F[1]=1, F[2]=-0.6949537938292681, \Theta[0]=0, \Theta[1]=-0.3541736065871279, \Phi[0]=0, \Phi[1]=-1.42603005254991\}, \tag{29}$$

In the fifth step, the direct substitution step is used to find the complement of missing real solutions. In addition, we get the following shape of solutions.

$$NSolve[u, u00, Reals] \tag{30}$$

And then results take the shape

$$f(\eta) = \eta - 0.6949537938292681\eta^2 + 0.024995582092212684\eta^3 + 0.0607551666481347\eta^4 - 0.025996755900233795 3\eta^5 - 0.004501152755274981\eta^6 + 0.00588534203037086\eta^7 - 0.0011191939983579483\eta^8 - 0.000783204981180159\eta^9 + 0.0004645273991077397\eta^{10}, \tag{31}$$

$$\theta(\eta) = \eta - 0.6949537938292681\,\eta^2 + 0.0448268706657643\eta^3 - 0.007232503345786588\eta^4 - 0.004222909475720365\eta^5 + 0.002100552974646337\eta^6 - 0.00005143889267233973\eta^7 - 0.0003440763402543985 7\eta^8 +$$

$0.0001114218302289403\eta^9 +$
$0.00001980285506127867\eta^{10},$ (32)

$\varphi(\eta) = -1.426203005254991\eta +$
$0.02073863468956536 2\eta^2 -$
$0.010923161902032368\eta^3 + 0.0011099875004928\eta^4 +$
$0.00247836901864159\eta^5 -$
$0.001080569888555436\eta^6 -$
$0.000022029173348652 24\eta^7 +$
$0.00020320015563752683\eta^8 -$
$0.00006117110032218832\eta^9 -$
$0.000013288479643649868\eta^{10}.$ (33)

When testing the accuracy of the solutions that we obtained from this step, we found that the solutions, in the beginning, are identical to the exact solution. Then the solutions deviate from the correct path. So it had to generalize of given results to get more accurate solutions in *the sixth step*

$\text{Table}[U[i] = \{\sum_{n=0}^{10} F_n h^n, \sum_{n=1}^{10} nF_n h^{n-1}, \frac{1}{2}\sum_{n=2}^{10} n(n-1)F_n h^{n-2}, \sum_{n=0}^{10} \Theta_n h^n, \sum_{n=1}^{10} n\Theta_n h^{n-1}, \sum_{n=0}^{10} \Phi_n h^n, \sum_{n=1}^{10} n\Phi_n h^{n-1}\}/.(\text{Join}[\text{NSolve}[u/.\text{qs}[i-1], \text{u00}], \text{qs}[i-1]]//\text{Flatten}), \{i, 1, 30\}],$
(34)

Solutions that are obtained after applying this algorithm are found to be accurate with the exact solution. In the next section, solutions that are compared with the nearest/ existing published results are given by Khan et al [24]. In addition, the solution of the present system of differential equations are offered in different two cases, the first in the case of base fluid at $W_e = 0$ and other in non-Newtonian fluid (Carreau fluid).

4 Results

This section is divided into four subsections formed and designed as follows: In the first subsection, the accuracy of presented results with recently published results by Khan et al [24] is proven/ verified through figures and table contents. The second subsection offers the distribution of velocity against penitent physical parameters to show the variance and physical meaning of increased fluid velocity. In the third subsection, the variance of physical parameters on the temperature and concentration profiles is studied.

4.1 Accuracy of Presented Results

It is common knowledge that to prove the effectiveness of a new method, we compare the graphs or tables obtained with recently published results by researchers recently. In the present article, results of velocity and temperature distributions are compared with existing published results by Khan et al, [24]. It found that the solutions computed by GDTM are in good agreement with the results given by the Rung-Kutta Fehlberg method. It is worth mentioning in Fig. 2 that the velocity profile is an increasing function at high values of the Hartmann number. Also, Fig. 3 shows that as usual large numbers of Prandtl numbers cause a rising in the temperature profile, [26].

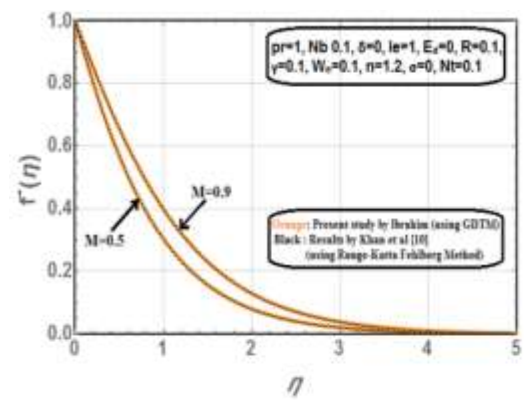

Fig. 2: Comparison of velocity behavior against Hartmann number [Present results versus Khan et al [24] results]

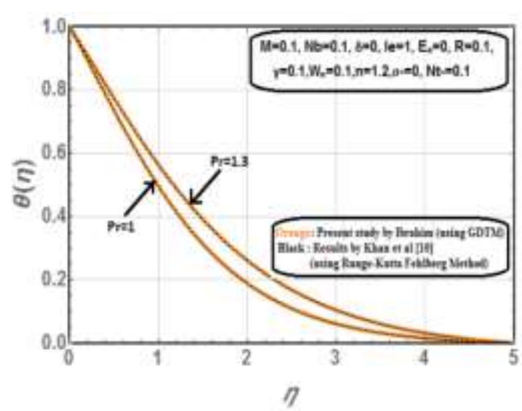

Fig. 3: Comparison of temperature profile against Prandtl number [Present results versus Khan et al [24] results]

Table 1 is representing a numerical comparison of Nusselt Number $-\theta'(\eta)$ values at different values of the Prandtl number. This comparison has been made with previously existing published results by Wang [25], Gorla and Sidawi, [26], Mabood et al [27], and Khan et al, [24], and found to be in good agreement. In addition, comparisons of temperature and concentration distributions have been made with results given by Khan et al, [24], and found to be excellent as stated/indicated in Table 2. It's worth mentioning that the standard values of parameters for all obtained figures are $P_r = 1, N_b = 0.2, M = 0.8, \delta = 0.1, N_t = 0.2,$ $E_a = 0.1, \beta = 0.4, m = 1, \gamma = 0.1, R = 0.3, Le =$ 0.1.

Table 1: Comparison of $-\theta'(0)$ at $M = \gamma = \lambda = L = N_t = N_b = \delta = \sigma = 0$ and $n = 1$

Table 1. numerical comparison of Nusselt Number $-\theta'(\eta)$ values at different values of the Prandtl number.

P_r	Khan et al **[24]**	Wang **[25]**	Gorla and Sidawi **[26]**	Mabod et al **[27]**	Present results
0.07	0.0645	0.0656	0.0656	0.0665	0.0655
0.20	0.1663	0.1691	0.1691	0.1691	0.1691
0.70	0.4554	0.4539	0.4539	0.4539	0.4534
2.00	0.9100	0.9114	0.9114	0.9114	0.9113
7.00	1.8929	1.8954	1.8905	1.8954	1.8903
20.00	3.3505	3.3539	3.3539	3.3539	3.3538
70.00	6.4598	6.4622	6.4622	6.4622	6.4627

Table 2. Comparison of $\theta(\eta)$ and $\varphi(\eta)$ (obtained resent results compared with given by Khan et al [24])

η	$\theta(\eta)$Khan et al [24]	$\theta(\eta)$ Present results	$\varphi(\eta)$ Khan et al [24]	$\varphi(\eta)$ Present results
0.0	1	1	1	1
0.7	0.787089028	0.787089028	0.87298093	0.872980938
1.4	0.582520232	0.582520232	0.746262989	0.746262989
2.1	0.407245275	0.407245275	0.612085865	0.612085865
2.8	0.265684286	0.265684286	0.469935625	0.322200746
3.5	0.155088686	0.155088686	0.322200746	0.322200746
4.2	0.070658319	0.070658319	0.171806533	0.171806533

4.2 Velocity Distribution Study

As stated above, the governing equations of the activation energy effects on nanofluid flow over a stretching sheet $Eqs. (8 - 10)$ are transformed and solved analytically using GDTM. The velocity gradient is graphically displayed by changing the values of the power index law β relation and Hartmann number M. It's depicted in Fig. 3 that the high values of the power index law cause an increase in stretching velocity, which creates supplementary deformation in the fluid. It can realize from Fig. 4 that the gradient of velocity diminishes by growing values of M, which causes the momentum boundary layer thickness to improve as upturns, whilst the dissimilarity in Lorentz force decreases the distribution of velocity.

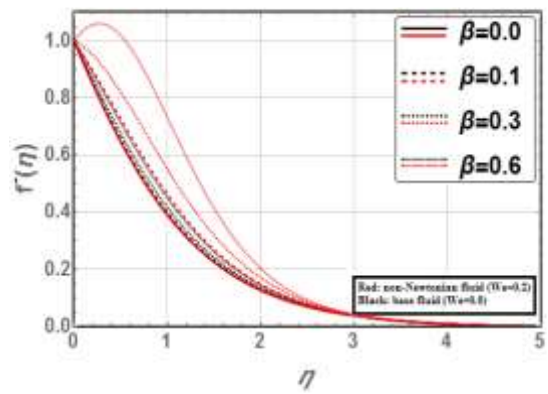

Fig. 4: Velocity behavior versus values β

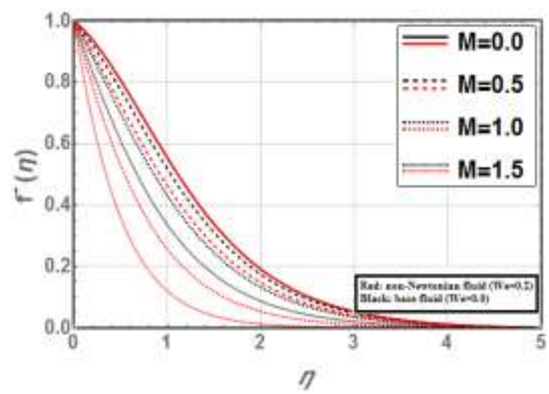

Fig. 5: Velocity behavior versus values M

4.3 Temperature and Concentration Study

Distributions of temperature and nanoparticle concentration are fully illustrated through this subsection versus different values of thermophoresis parameter (N_t) thermal radiation parameter (R) , chemical reaction species (σ), power index law parameter (β), Hartmann number (M) and activation parameter (E_a) in Figs. 6-17. It's visualized from Figs. 6 and 7 that the temperature gradients are growing at high values of N_t and R. *Noticeably*, thermophoresis and thermal radiation parameters acquire the fluid particle more energy making the temperature have high values, [24] and [27]. As expected, the temperature distribution is a decreasing function on σ, β, M and E_a by looking at their definitions. So, Figs. 8-10 are depicted to approve that the high values of σ, β, M and E_a reduce the fluid temperature. In addition, chemical reaction and activation energy parameters do not directly affect on temperature of fluid accordingly, the effect is not clear as found in the case of the power index law parameter and Hartmann number [11], [12]. All results show that the influences of physical parameters on the distribution of temperature become more sight in non-Newtonian fluid than found in the base fluid.

Nanoparticle concentration distribution have usually a contradictory behavior to temperature distribution with the same parameters, as the inverse relationship between them. However, it should be noted from Figs. 12-13 that the concentration of fluid diminutions at high values of R and M actually as in [25] and [26]. Whilst, the concentration and temperature distributions are considered to have an increasing function in thermophoresis parameter N_t [27], as seen in Figs. 6 and 14. In addition, Figs. 15-17 show that the fact of nanoparticle concentration distribution rises at high values of σ, β and E_a.

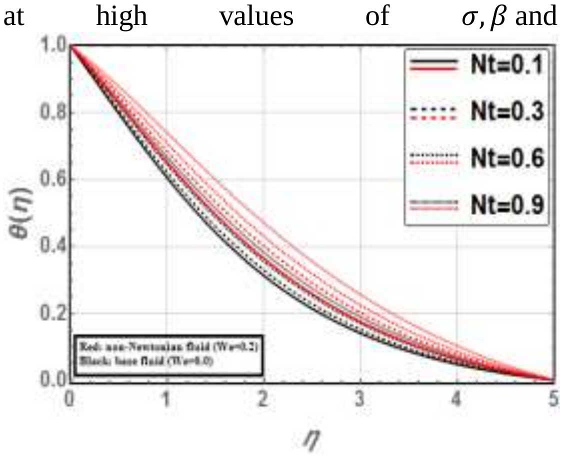

Fig. 6: Temperature behavior versus values of Nt.

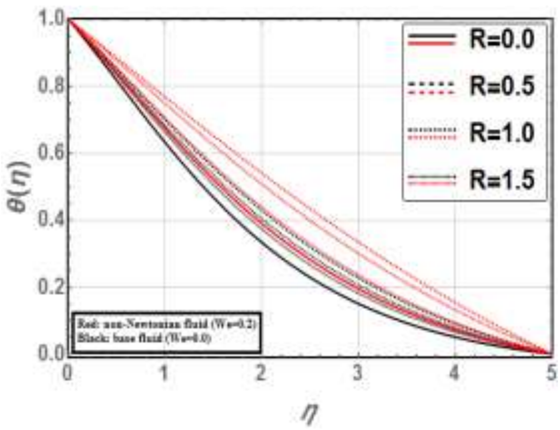

Fig. 7: Temperature behavior versus values of R.

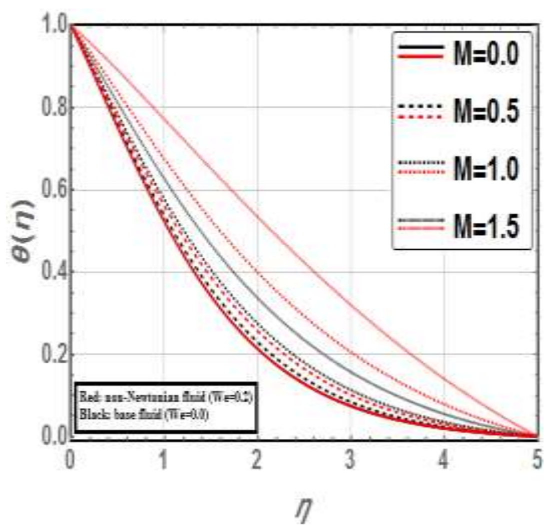

Fig. 8: Temperature behavior versus values of M.

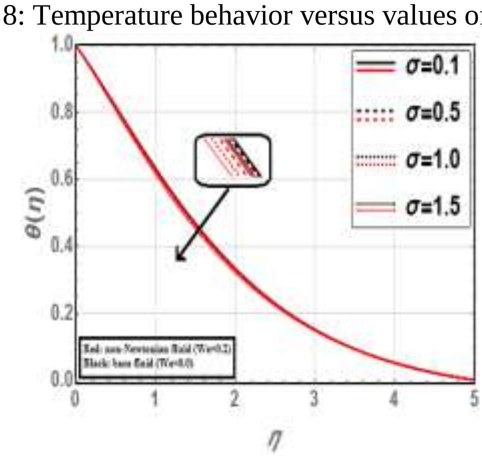

Fig. 9: Temperature behavior versus values of σ.

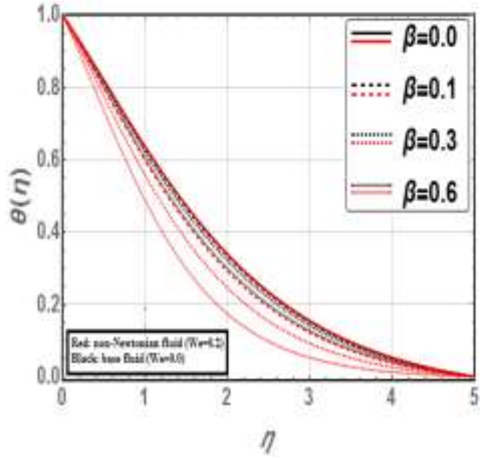

Fig. 10: Temperature behavior versus values of β.

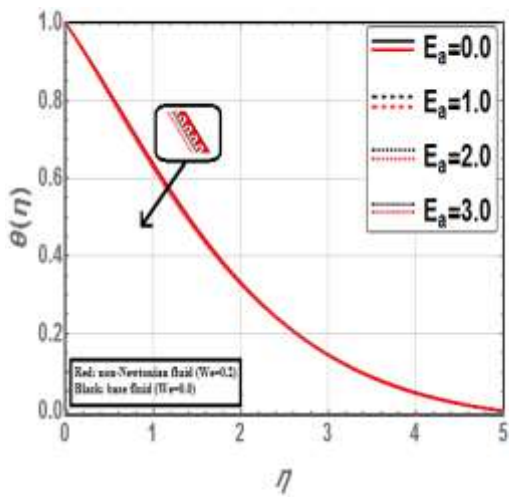

Fig. 11: Temperature behavior versus values of E_a.

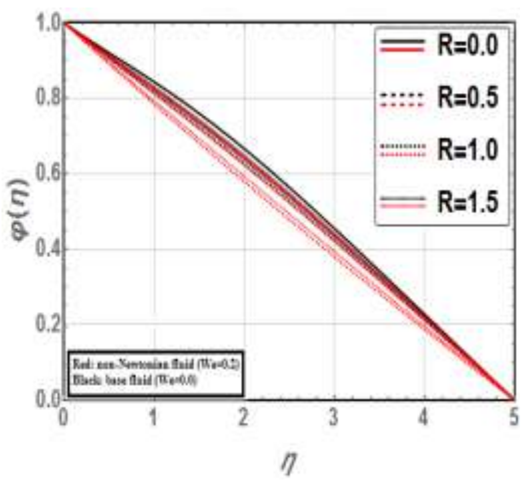

Fig. 12: Concentration behavior versus values of R.

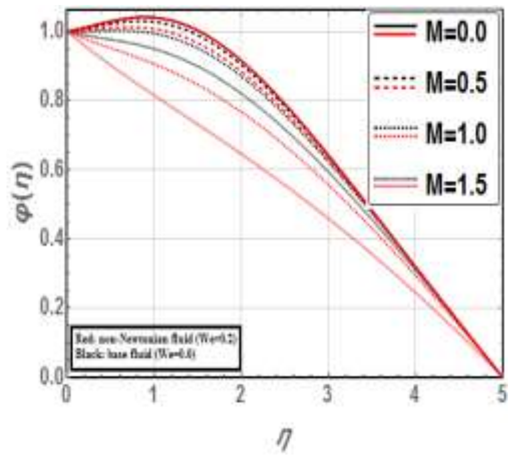

Fig. 13: Concentration behavior versus values of M.

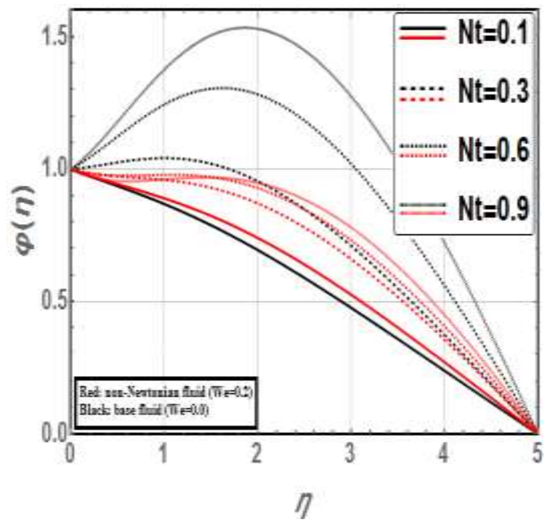

Fig. 14: Concentration behavior versus values of Nt.

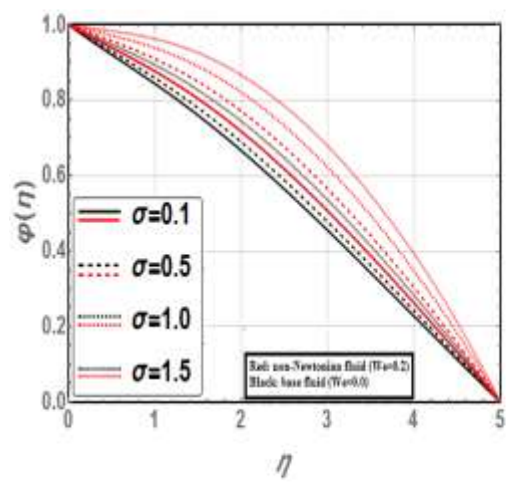

Fig. 15: Concentration behavior versus values of σ.

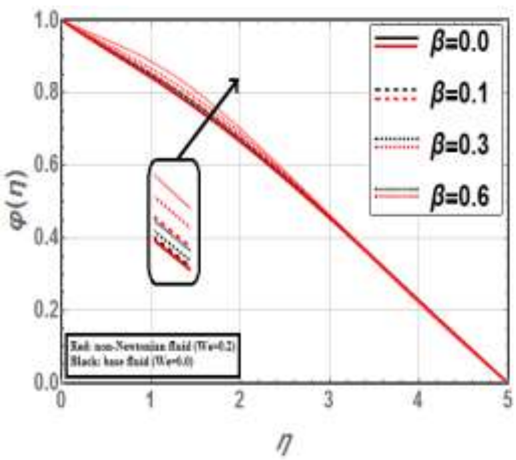

Fig. 16: Concentration behavior versus values of β.

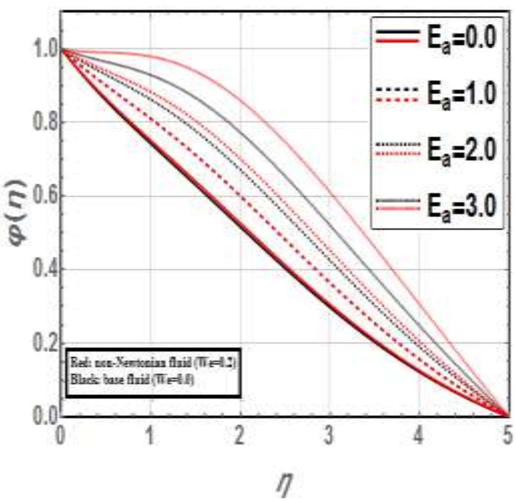

Fig. 17: Concentration behavior versus values of E_a.

5 Conclusion

In this article, a semi-analytical solution to the MHD Boundary layer of Carreau nanofluid is computed using the generalized differential transform method. Entropy generation, activation energy, and variable thickness sheet are taken into consideration. Combined solutions of the proposed model in the cases of Newtonian and non-Newtonian fluid are discussed to clarify the fluid behaviors. The obtained solution is compared with those of Wang. [25], Gorla and Sidawi. [26], Mabood et al. [27], and Khan et al . [24], and a good agreement was found. Activation energy and thermal radiation effects are considered. The main outcomes of the present study can be conceived as follow:

- Analytical methods like GDTM are the best way to get more accurate solutions of fluid models without linearization or perturbation assumptions.
- The distribution of velocity growths at high values of power index law relation.
- This fluid model can be applied in solar energy power generation, ethylene glycol, nuclear reactions, etc.
- High values of activation energy increase the concentration distribution.
- GDTM is an effective method for solving a highly non-linear system of differential equations.
- Thermal radiation has opposite effects on the distributions of temperature and concentration.
- Power index law relation and Hartmann number have to contradict influences on the velocity distribution.

References:

[1] S. E. Ghasemi and M. Hatami , Solar radiation effects on MHD stagnation point flow and heat transfer of a nanofluid over a stretching sheet, *Case Studies in Thermal Engineering*, Vol. 25, 2021, 100898.

[2] M. Khan, M.Y. Malik and T. Salahuddin, Heat generation and solar radiation effects on Carreau nanofluid over a stretching sheet with variable thickness: Using coefficients improved by Cash and Carp, *Results in Physics*, Vol. 7, 2017, pp. 2512–2519.

[3] A. Shafiq and T. N. Sindhu, Statistical study of hydromagnetic boundary layer flow of Williamson fluid regarding a radiative surface, *Results in Physics*, Vol. 7, 2017, pp. 3059-3067.

[4] F. Mabood, A. Shafiq, W. A. Khan, I. A. Badruddin, MHD and nonlinear thermal radiation effects on hybrid nanofluid past a wedge with heat source and entropy generation, *International Journal of Numerical Methods for Heat & Fluid Flow*, Vol. 32, No.1, 2021, pp. 1-18.

[5] A. Shafiq, G. Rasool, H. Alotaibi, H. M. Aljohani, A. Wakif, I. Khan and S. Akram, Thermally Enhanced Darcy-Forchheimer Casson-Water/Glycerine Rotating Nanofluid Flow with Uniform Magnetic Field, *Micromachines*, Vol. 12, No. 6, 2021, 605.

[6] I. Zari, A. Shafiq, T. S. Khan and S. Haq, Marangoni Convective Flow of GO-kerosene- and GO-water-based Casson Nanoliquid Toward a Penetrable Riga Surface, *Brazilian Journal of Physics*, Vol. 51, 2021, pp.1747–1762.

[7] M. Y. Malik, K. Imad, H. Arif and T. Salahuddin. Mixed convection flow of MHD Eyring-Powell nanofluid over a stretching sheet: a numerical study, *AIP Adv*., Vol. 5, 2015, 117118.

[8] Hanaa Abdel Hameed Asfour and M. G. Ibrahim, Numerical simulations and shear stress behavioral for electro-osmotic blood flow of magneto Sutterby nanofluid with modified Darcy's law, *Thermal Science and Engineering Progress*, Vol. 37, No. 1, 2023, 101599.

[9] M. G. Ibrahim and Mohamed Abouzeid, Influence of variable velocity slip condition and activation energy on MHD peristaltic flow of Prandtl nanofluid through a non-uniform channel, *Scientific Reports*, Vol. 12, No. 1, 2022.

[10] M. G. Ibrahim, Computational calculations for temperature and concentration-dependent density effects on creeping motion of Carreau fluid: biological applications, *Waves in Random and Complex Media*, Vol. 32, 2022.

[11] M. G. Ibrahim, N. A. Fawzy, Arrhenius energy effect on the rotating flow of Casson nanofluid with convective conditions and velocity slip effects: Semi-numerical calculations, *Heat Transfer*, Vol. 55, 2022.

[12] M. G. Ibrahim, Adaptive Computations to Pressure Profile for Creeping Flow of a Non-Newtonian Fluid With Fluid Nonconstant Density Effects, *Journal of Heat Transfer-Transactions of the ASME*, Vol. 144, No. 10, 2022, 103601.

[13] M. G. Ibrahim, Concentration-dependent electrical and thermal conductivity effects on magnetoHydrodynamic Prandtl nanofluid in a divergent–convergent channel: Drug system applications, *Proc IMechE Part E: J Process Mechanical Engineering*, 2022: 0749.

[14] M. G. Ibrahim, Adaptive simulations to pressure distribution for creeping motion of Carreau nanofluid with variable fluid density effects: Physiological applications, *Thermal Science and Engineering Progress*, Vol. 32, No. 1, 2022, 101337.

[15] L. Prandtl and Verhandlung des III Internationalen Mathematiker Kongresses (Heidelberg, 1904), pp. 484-491.

[16] S. A. Pasha, Y. Nawaz and M. S. Arif, A third-order accurate in time method for boundary layer flow problems, *Applied Numerical Mathematics*, Vol. 161, 2021, pp. 13–26.

[17] M. Khan, M.Y. Malik and T. Salahuddin, Heat generation and solar radiation effects on Carreau nanofluid over a stretching sheet with variable thickness: Using coefficients improved by Cash and Carp, *Results in Physics*, Vol. 7, 2017, 2512–2519.

[18] T. Salahuddin, A. M. Bashir, M. Khan and Y. Elmasry, Activation energy study for peristaltically driven divergent flow with radiation effect, *Case Studies in Thermal Engineering*, Vol. 27, 2021, 101172.

[19] Z. Shafique, M. Mustafa and A. Mushtaq, Boundary layer flow of Maxwell fluid in rotating frame with binary chemical reaction and activation energy, *Results in Physics*, Vol. 6, 2016, pp. 627-633.

[20] R. J. P. Gowda, R. N. Kumar, A. M. Jyothi, B. C. kumara and L. E. Sarris, Impact of binary chemical reaction and activation energy on heat and mass transfer of marangoni driven boundary layer flow of a non-Newtonian nanofluid, *Processes*, Vol. 9, 2021, 702.

[21] D. Borah and M.K. Baruah, Proposed novel dynamic equations for direct determination of activation energy in non-isothermal isothermal systems, Fuel processing technology, Vol. 86, 2005, pp. 781-794.

[22] J. Wang, and R. Raj, Estimate of the Activation Energies for Boundary Diffusion from Rate-Controlled Sintering of Pure Alumina, and Alumina Doped with Zirconia or Titania, Journal of the American Ceramic Society, Vol. 73, No. 5, 1990, 1172.

[23] A. Kiraci, H. Yurtseven, Temperature Dependence of the Raman Frequency, Damping Constant and the Activation Energy of a Soft-Optic Mode in Ferroelectric Barium Titanate. *Ferroelectrics*, Vol. 432, 2012, pp. 14–21.

[24] M. Khan, M.Y. Malik and T. Salahuddin, Heat generation and solar radiation effects on Carreau nanofluid over a stretching sheet with variable thickness: Using coefficients improved by Cash and Carp, *Results in Physics*, Vol. 7, 2017, pp. 2512–2519.

[25] C.Y. Wang, Free convection on a vertical stretching surface, *Journal of Applied Mathematics and Mechanics*, Vol. 69, 1989 418–420.

[26] R.S.R. Gorla, I. Sidawi, Free convection on a vertical stretching surface with suction and blowing, *Journal of Applied Sciences Research*, Vol. 52, 1994, pp. 247–257.

[27] F. Mabood, W. A. Khan and A. I. M. Ismail, MHD boundary layer flow and heat transfer of nanofluids over anonlinear stretching sheet: a numerical study, *Journal of Magnetism and Magnetic Materials*, Vol. 374, 2015, pp. 569–576.

[28] Y. M. Chu, M. I. Khan, Niaz B. Khan, S. Kadry, S.U. Khan, I. Tlili and M.K. Nayak, Significance of activation energy, bio-convection and magnetohydrodynamic in flow of third grade fluid (non-Newtonian) towards stretched surface: A Buongiorno model analysis, *International communications in heat and mass transfer*, Vol. 118, 2020, 104893.

[29] J. K. Zhou, Differential transformation and its applications for electrical Circuits, Huazhong University Press, *Wuhan, China*, (in Chinese), 1986.

[30] Z.M. Odibat, Cyrille Bertelle and M. A. Aziz Alaoui, Gérard H.E. Duchamp, A multistep differential transform method and application to non-chaotic or chaotic systems, *Computers Mathematics with Applications*, Vol. 59, 2010, pp. 1462–1472.

[31] M. G. Ibrahim and Hanaa A. Asfour, The effect of computational processing of temperature- and concentration-dependent parameters on non-Newtonian fluid MHD: Applications of numerical methods, *Heat Transfer*, Vol. 51, No. 1, 2022, pp. 1-18.

[32] M. G. Ibrahim, Concentration-dependent viscosity effect on magnetonano peristaltic flow of Powell-Eyring fluid in a divergent-convergent channel, *International Communications in Heat and Mass Transfer*, Vol. 134, No. 2, 2022, 105987.

[33] M. G. Ibrahim, Numerical simulation to the activation energy study on blood flow of seminal nanofluid with mixed convection effects, *Computer Methods in Biomechanics and Biomedical Engineering*, Vol. 25, 2022, pp. 1-13.

[34] M. G. Ibrahim, Numerical simulation for non-constant parameters effects on blood flow of Carreau–Yasuda nanofluid flooded in gyrotactic microorganisms: DTM-Pade application, *Archive of Applied Mechanics*, Vol. 92, No. 5, 2022, pp. 1-12.

[35] M. G. Ibrahim, W. M. Hasina and A. A. ElShekhipy, Instantaneous influences of thermal radiation and magnetic field on peristaltic transport of Jeffrey nanofluids in a tapered asymmetric channel: Radiotherapy of oncology treatment, *Advances, and Applications in Fluid Mechanics*, Vol. 24, No.1-2, 2021, pp. 25-55.

[36] W. M. Hasona, A.A. El-Shekhipy, M.G. Ibrahim, Combined effects of magnetohydrodynamic and temperature-dependent viscosity on peristaltic flow of Jeffrey nanofluid through a porous medium: Applications to oil refinement, *International Journal of Heat and Mass Transfer*, Vol. 126, 2018, 700–714.

[37] M. G. Ibrahim, W.M. Hasona and A.A. ElShekhipy, Concentration-dependent viscosity and thermal radiation effects on MHD peristaltic motion of Synovial Nanofluid: Applications to rheumatoid arthritis treatment, *Computer Methods and Programs in Biomedicine*, Vol. 170, 2019, pp. 39–52.

[38] W. Hasona, Nawal H. Almalki, Abdelhafeez A. El-Shekhipy and M. G. Ibrahim, Combined Effects of Variable Thermal Conductivity and Electrical Conductivity on Peristaltic Flow of Pseudoplastic Nanofluid in an Inclined Non-Uniform Asymmetric Channel: Applications to Solar Collectors, *Journal of Thermal Science and Engineering Applications*, Vol. 12, No. 2, 2020, 021018.

[39] W. M. Hasona, A. El-Shekhipy and M. G. Ibrahim, Semi-analytical solution to MHD peristaltic flow of a Jeffrey fluid in presence of Joule heat effect by using Multi-step differential transform method, *New Trends In Mathematical Science*, Vol. 7, 2019, pp. 123-137.

[40] W. M. Hasona, N. H. Almalki, A. A. ElShekhipy, M. G. Ibrahim, Thermal radiation and variable electrical conductivity effects on MHD peristaltic motion of Carreau nanofluids: Radiotherapy and thermotherapy of oncology treatment, *Heat Transfer—Asian Res.*, Vol. 55, 2019, pp. 1-19.

[41] W. Hasona, N. Al-Malki, A. A. El-Shekhipy, and M. G. Ibrahim, Combined Effects of Thermal Radiation and Magnetohydrodynamic on Peristaltic Flow of Nanofluids: Applications to Radiotherapy and Thermotherapy of Cancer, *Current NanoScience*, Vol. 16, No. 1, 2020, pp. 121-134.

[42] Hana Abdelhameed Asfour and M. G. Ibrahim, Numerical simulation for SI model with variable-order fractional, *New Trends in Mathematical Sciences*, Vol. 4, 2016, 45-55.

[43] A. A. M. Hassan, S. A. Hoda Ibrahim, Amr M. S. Mahdy and M.G. Ibrahim, A new solution of SIR model by using the differential fractional transformation method, *International Journal of Engineering and Applied Science*, Vol. 4, No. 11, 2014, pp. 12-22.

[44] W. M. Hasona, A.A. El-Shekhipy and M. G. Ibrahim, Computational simulation for the analytical and numerical treatment related to SIRs models, *IOSR Journal of Mathematics*, Vol. 14, No. 4, 2018, pp. 81-91.

Conflict of Interest

The authors declared that there is no conflict of interest

Contribution of Individual Authors to the Creation of a Scientific Article (Ghostwriting Policy)

M.G. Ibrahim: Conceptualization, Methodology, Software, Data duration, Writing – original draft, Hanaa Abdel Hameed Asfour: Visualization, Investigation, Validation, Writing – review & editing.